Effect of inhomogeneities and substrate on the dynamics of the metal-insulator transition in VO_2 thin films

M. Rodriguez-Vega,[1] M. T. Simons,[1] E. Radue,[1] S. Kittiwatanakul,[2] J. Lu,[2] S. A. Wolf,[3,2] R. A. Lukaszew,[1] I. Novikova,[1] and E. Rossi[1]

[1]*Department of Physics College of William and Mary, Williamsburg, Virginia 23187, USA*

[2]*Department of Material Science, University of Virginia, Charlottesville, Virginia 22904, USA*

[3]*Department of Physics, University of Virginia, Charlottesville, Virginia 22904, USA*

(Received 9 May 2015; revised manuscript received 16 July 2015; published 11 September 2015)

We study the thermal relaxation dynamics of VO_2 films after the ultrafast photoinduced metal-insulator transition for two VO_2 film samples grown on Al_2O_3 and TiO_2 substrates. We find two orders of magnitude difference in the recovery time (a few nanoseconds for the VO_2/Al_2O_3 sample versus hundreds of nanoseconds for the VO_2/TiO_2 sample). We present a theoretical model to take into account the effect of inhomogeneities in the films on the relaxation dynamics. We obtain quantitative results that show how the microstructure of the VO_2 film and the thermal conductivity of the interface between the VO_2 film and the substrate affect long time-scale recovery dynamics. We also obtain a simple analytic relationship between the recovery time-scale and the film's parameters.

DOI: 10.1103/PhysRevB.92.115420 PACS number(s): 68.55.−a, 64.70.K−, 78.20.Bh

I. INTRODUCTION

Vanadium dioxide (VO_2) undergoes a metal-insulator transition (MIT) around room temperature [1] enabling a wide range of potential applications. It has recently been shown that it is possible to photoinduce the insulator-to-metal transition in VO_2 in the subpicosecond time scale [2–8]. This finding makes VO_2 a material of great interest for electronic and photonic applications, such as ultrafast switches or transistors. The realization of VO_2-based switches requires the ability to control the VO_2 MIT dynamics using external fields, as well as a better understanding of the recovery mechanisms after the external field is turned off and the material returns to its normal state. The mechanism by which the photoinduced insulator-to-metal takes place in VO_2 is still not fully understood due to the complexity of the electronic behavior of VO_2 arising from the presence of strong electron-lattice coupling and electron-electron interactions [9–12]. As a result, VO_2 is a unique material of great fundamental and practical interest.

At low temperatures ($T \lesssim 340$ K), the VO_2 lattice has a monoclinic structure, whereas at high temperatures ($T \gtrsim 340$ K) it has a tetragonal structure. This difference in lattice structure is reflected in the band structure: VO_2 is an insulator in the monoclinic phase and a metal in the tetragonal phase. This simple picture is complicated by the fact that in VO_2 electron-electron correlations are very strong and can provide an important contribution to the localization of the electronic states via the Mott mechanism [10,11,13,14]. It appears that a full account of the MIT must take into account the interplay of the lattice dynamics and the electron dynamics driven by strong electron-electron interactions. This is a fascinating and extremely challenging problem that in addition is complicated by the unavoidable presence of inhomogeneities [15,16].

Several works [6,17–25] have investigated the short time-scale dynamics after the photoinduced transition. In particular, Ref. [26] presented a comparison of the long time-scale recovery dynamics between VO_2 films on a crystal substrate or a glass substrate and found that the recovery time for the films on the glass substrate was much longer than for the films on a crystal substrate. The recovery time was modeled using the heat equation to describe the heat flow across the interface between the VO_2 film and the substrate. The difference in the characteristic time between the two types of substrates was attributed to the fact that the thermal conductivity of the interface was expected to be much smaller for glass substrates than for crystal substrates.

In this work, we present a theory to properly take into account the effect of inhomogeneities on the recovery dynamics of VO_2 films. Our theory describes simultaneously: (i) the profile of the reflectivity across a thermal induced MIT; (ii) the long time-scale recovery dynamics of the reflectivity after a photoinduced insulator-to-metal transition; (iii) the observed difference of two orders of magnitude between samples with different substrates. Inhomogeneities are due to the fact that the film is comprised of grains with different sizes and different local properties, such as strain [27,28] and chemical composition.

The presence of inhomogeneities induces a distribution of values for the transition temperature T_c within the film. To take this into account, we derive a generalized heat equation that includes the fact that during the recovery from the photoinduced insulator-to-metal transition, at any given time, a fraction of the sample is undergoing the metal-to-insulator transition, another fraction is still cooling in the metallic phase, and another fraction is already cooling in the insulating phase. A key ingredient of the generalized heat equation is the correct description of the time evolution of the fraction of the sample that is metallic, insulating, or undergoing the phase transition. We then use our theoretical model to obtain the scaling relation between the characteristic recovery time τ and the parameters of the films. Our theoretical model, and the underlying assumptions, are strongly supported by our experimental results. Differently than in Ref. [26], our VO_2 films have all crystal substrates, no glass. Yet, we find that τ can be more than two orders of magnitude different depending on the crystal substrate, TiO_2 or Al_2O_3, Fig. 1.

The generalized heat equation (9), which properly takes into account the effect of the films inhomogeneities on the recovery dynamics, is the main result of our work. Our theory

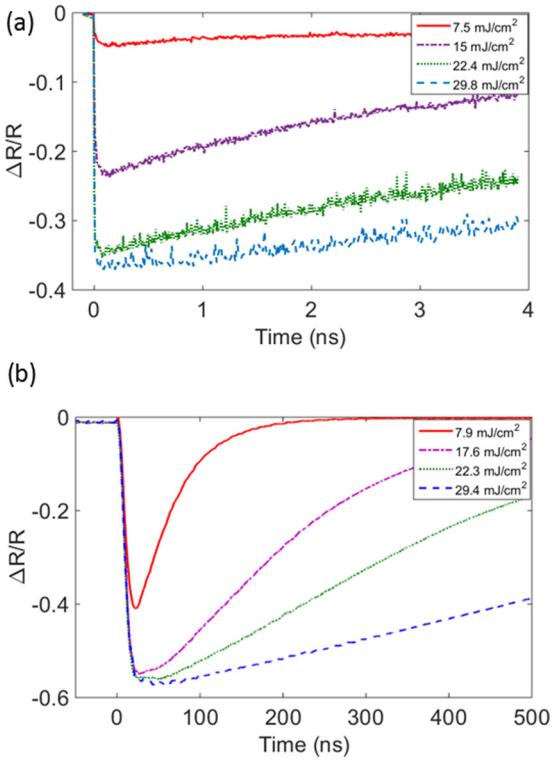

FIG. 1. (Color online) Relative change in reflectivity ($\Delta R/R$) for the VO_2 film on (a) Al_2O_3 substrate and (b) TiO_2 substrate as a function of time after the MIT is induced at time $t = 0$ by a strong ultrafast pump pulse. The values of the pump fluence are shown in the legend, and the sample temperature is set to (a) 311 and (b) 280 K, which correspond to approximately 30 K below the critical temperature T_c for thermally induced MIT for each sample.

allows the description of the recovery dynamics consistently with the measurements obtained for the thermally driven MIT. The scaling between the characteristic recovery time τ and the parameters of the film is another important result of our work.

Our work is relevant to the more general problem of how spatial inhomogeneities affect a first-order phase transition. The ability of our treatment to contribute to this general problem relies on the fact that in VO_2 the two phases across the first-order phase transition have very different electronic properties (metallic versus insulating behavior) that allows us to get an accurate phase mapping, via optical reflectivity measurement, of the time evolution of the metallic (insulating) fraction and, indirectly, of the spatial inhomogeneities present during the transition.

The work is organized as follows. Section II describes the experimental arrangements to measure the optical reflectivity time evolution. The details of the theoretical model that we use to characterize the distribution of the films' inhomogeneities and the long-time dynamics of the reflectivity after a photoinduced insulator-to-metal transition are presented in Secs. III and IV, respectively. In Sec. V, we demonstrate how the variations in statistical properties of the two films result in a significant difference in the relaxation time scales, and in Sec. VI, we provide our conclusions.

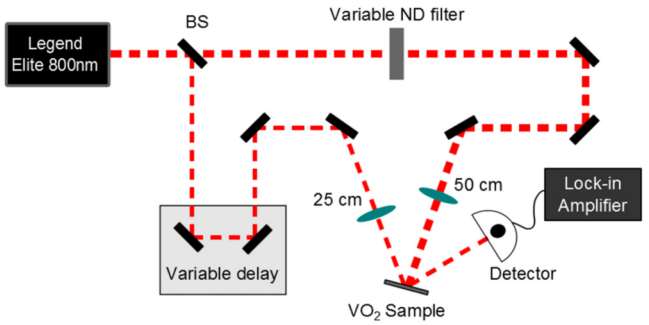

FIG. 2. (Color online) Schematic of the ultrafast pump-probe setup. BS is an 80/20 beam splitter.

II. EXPERIMENTAL SETUP

In our experiments, we studied two VO_2 thin-film samples, both of which were produced using reactive-bias target ion beam deposition (RBTIBD) [29]. One sample was grown on 0.5-mm-thick c-Al_2O_3, and the thickness of the VO_2 film was 80 nm. The other sample was grown on a 0.5-mm-thick TiO_2 (011) substrate, and was measured to be 110-nm thick. X-ray diffraction (XRD) evaluation of both films showed them to be crystalline, and detailed characterization information is available in previous reports [30,31].

For the photoinduced insulator-to-metal transition experiments, we used an ultrafast laser system (Coherent Mantis oscillator and Legend Elite regenerative amplifier) with approximately 100-fs pulses with a central wavelength at 800 nm and a repetition rate of 1 kHz. The properly attenuated output of the laser was split into strong pump pulses and weaker probe pulses using a beam splitter in a standard pump-probe configuration, shown in Fig. 2. The more powerful pump beam, focused to a 180-μm-diameter spot on the surface of the sample, was used to induce the insulator-to-metal transition, and its fluence was controlled using a variable neutral-density filter (VF). The fluence of the probe beam was further attenuated to a value well below the insulator-to-metal threshold ($\phi_{\text{probe}} \leqslant 100\ \mu\text{J/cm}^2$), and we used its reflectivity from the sample to monitor the instantaneous optical properties of the VO_2 film. The probe pulses were directed along a variable delay stage to accurately control the relative timing between the pump and probe pulses by up to 4 ns with a few fs precision. The probe beam was focused on the sample at the same spot as the pump beam, using a shorter focal length lens. When tuned to the center of the pump beam focal spot, the smaller probe beam diameter (90 μm) ensured probing a region of uniform pump intensity.

The reflected probe power was measured using a silicon photodetector, and further analyzed using a lock-in amplifier. To minimize the effects of probe pulse instabilities, as well as long-terms drifts due to environmental changes, we report the relative change in probe reflection $\Delta R/R$ with the pump beam on or off.

Notably, the MIT relaxation of the VO_2/TiO_2 sample was not measurable with the femtosecond probe, as its characteristic decay time exceeded the 4-ns maximum pulse separation, determined by the length of the delay stage. To measure the relaxation of the metallic VO_2 grown on the rutile

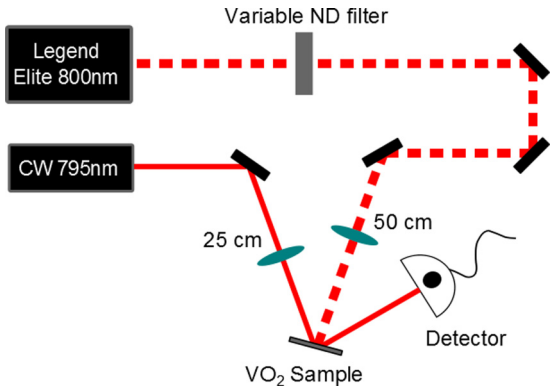

FIG. 3. (Color online) Schematic of the experimental setup using a continuous-wave probe laser.

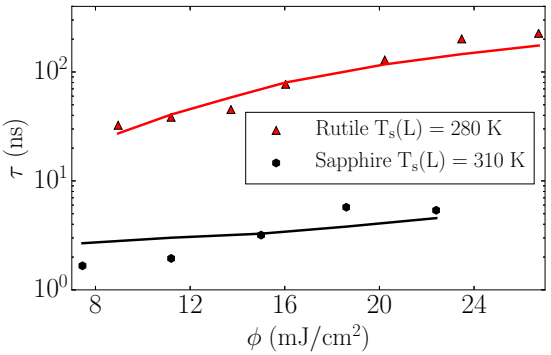

FIG. 4. (Color online) Dependence of metal state decay constant τ on the laser pump fluence and substrate temperature. Dots represent experimental data and lines correspond to the results of the theoretical calculations. The initial temperature T_s for both sample substrates was approximately 30 K below their respective MIT critical temperatures.

sample, we modified our experimental setup by replacing the femtosecond probe pulses with a continuous-wave (CW) diode laser operating at 785 nm and a fast photodiode (measured response time of approximately 10 ns), as shown in Fig. 3. This detection method allowed us to measure changes in reflectivity for times longer than ≈20 ns after the insulator-to-metal transition, that were inaccessible with the femtosecond probe arrangement.

Figure 1 shows sample measurements of both the VO_2/Al_2O_3 and VO_2/TiO_2 films, using the femtosecond and CW probe arrangements, respectively. The overall reflectivity depends on the refractive index of both the film and the substrate, and the refractive indices of TiO_2 and Al_2O_3 are different. Because it is easier to average the CW laser reflection signal, the curves for VO_2/TiO_2 are smoother than the curves for the VO_2/Al_2O_3. The rutile reflection spectra recorded using the ultrafast probe had the same noise as for the sapphire samples, indicating that the differences in the noise are due to differences in the probes, not in the samples.

For values of the pump fluence higher than a threshold, which depends on the substrate temperature, we can see that the reflectivity, soon after the pump pulse, remains almost constant for some time, i.e., its dynamics exhibits a "flat" region, see in particular Fig. 1(b). The observed "flattening" of the curves is due to the pump pulse heating the sample to a temperature above the threshold value for the thermally induced insulator-to-metal transition [23,25]. In this case, the reflectivity stays unchanged at the level corresponding to a fully metallic phase until a non-negligible fraction of the sample cools down to the transition temperature. For all experimental curves, only the later exponential part of the measured reflectivity was included into the fitting thermal relaxation time analysis.

The analysis of the relative reflectivity for both VO_2 samples demonstrates that after the initial rapid change during the ultrafast insulator-to-metal transition, its time evolution during the recovery is well fitted by a single exponential function with a recovery time constant τ:

$$R_{\text{fit}}(t) = R_I + (R_0 - R_I)e^{-t/\tau}, \quad (1)$$

where R_I corresponds to the reflectivity in the insulating phase, and R_0 corresponds to the reflectivity at $t = 0$ s. The results of such measurements are shown in Fig. 4: for VO_2/Al_2O_3 films, we obtained values of τ of the order of few nanoseconds, whereas it took the VO_2/TiO_2 sample a few hundred nanoseconds to relax back to the insulating state. This two orders of magnitude difference in the recovery times was even more surprising considering that the characteristic times for the transition itself were quite similar, as demonstrated in previous studies [25]. In the discussion below, we demonstrate that the relaxation dynamics strongly depends on the microstructure of the VO_2 films, which in turn is strongly influenced by the properties of the substrate and their interface. Figure 4 also reveals that the rate of thermal relaxation for both samples increases with higher pump power.

III. THEORETICAL MODELING OF INHOMOGENEITIES

In order to take into account the effect of the inhomogeneities on the MIT dynamics, the first step is to characterize them. To do this, we can use the profile of the reflectivity across the thermally induced MIT. The dotted lines in Figs. 5(a) and 5(b) show the measured reflectivity as a function of temperature across the thermally induced MIT for a VO_2 film grown on sapphire and TiO_2, respectively. The temperature

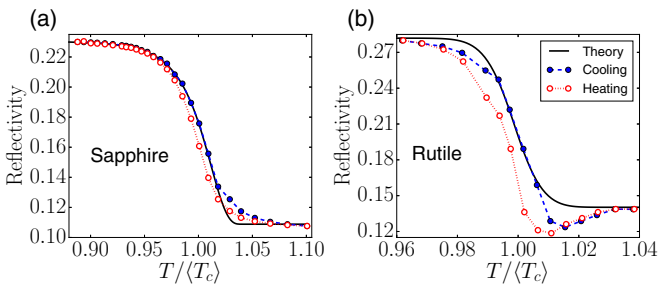

FIG. 5. (Color online) Evolution of the reflectivity across the thermally induced MIT for the case of sapphire and rutile substrates normalized to the average critical transition temperature. The open circles (red) correspond to the measured reflectivity in the heating branch, the solid circles (blue) correspond to the measured reflectivity in the cooling branch, and the solid curve corresponds to the theoretical result. For rutile substrate $\langle T_c \rangle = 314.0$ K, and for the sapphire substrate $\langle T_c \rangle = 340.1$ K.

driven MIT in VO_2 is a first-order transition. In the ideal case, the reflectivity is expected to exhibit a finite, steplike change at the critical temperature T_c, at which the sample goes from a low-temperature insulating state to a high-temperature metallic state. In thin films, however, the optical reflectivity smoothly changes from the value corresponding to the insulating phase (R_I) to the value characteristic to the metallic phase (R_M) as the temperature increases, as Fig. 5 illustrates. For our samples, the hysteresis loop is very narrow [31]. The fact that the MIT takes place over a range of temperatures implies that different regions of the sample have different values of T_c. This is different from the case of an ideal, homogeneous system for which the whole sample exhibits the coexistence of metallic and insulating regions only for $T = T_c$. As a consequence the MIT in the films is characterized not by a single critical temperature but by a distribution $P(T_c)$ of critical temperatures. This is due to the fact that the VO_2 films are inhomogeneous: they are formed by crystal grains with different local properties. Different grains in general have different sizes, slightly different stoichiometry, and experience different local strains. It is very challenging to characterize the distribution of all the local properties that can affect the transition temperature of each grain. However, for our purposes, we only need $P(T_c)$ and, as we show below, this can obtained directly from the profiles of $R(T)$ without having to characterize the distribution of the local properties affecting T_c. Let η_I be the fraction of the sample in the insulating phase. At a given temperature T, we have

$$\eta_I(T) = \int_T^\infty P(T_c) dT_c. \tag{2}$$

Let $\eta_m(T) = 1 - \eta_I(T)$ be the fraction of the film in the metallic phase. To obtain the evolution of $\eta_I(T)$ across the MIT, and therefore $P(T_c)$, considering that changes in the fraction of the film that is metallic (insulating) are the dominant cause of changes in the reflectivity, we can use a two-fluid effective medium theory (EMT) [32–35]. In the EMT, the inhomogeneous system is replaced by an effective homogeneous medium having the same, bulk, electric properties. Let ϵ_M, ϵ_I be the dielectric constants (at the probing frequency) of VO_2 in the metallic and insulating phase, respectively. Then, the dielectric constant of the effective medium, ϵ_{EMT}, is given by the following equation:

$$\frac{\eta_I(\epsilon_I - \epsilon_{\mathrm{EMT}})}{\epsilon_{\mathrm{EMT}} + g(\epsilon_I - \epsilon_{\mathrm{EMT}})} + \frac{\eta_M(\epsilon_M - \epsilon_{\mathrm{EMT}})}{\epsilon_{\mathrm{EMT}} + g(\epsilon_M - \epsilon_{\mathrm{EMT}})} = 0. \tag{3}$$

In Eq. (3), g is a factor that depends on the shape of the grain. Without loss of generality, we set $g = 1/3$. Let n and k be the real and imaginary parts, respectively, of the index of refraction, so that for the effective medium $n + ik = \sqrt{\epsilon_{\mathrm{EMT}}}$ and therefore

$$R = \left| \frac{\cos\theta_0 - \sqrt{(n+ik)^2 - \sin^2\theta_0}}{\cos\theta_0 + \sqrt{(n+ik)^2 - \sin^2\theta_0}} \right|^2, \tag{4}$$

where $\theta_0 \approx 15^\circ$ corresponds to the probe incidence angle. Given our experimental setup, we can reliably obtain the imaginary part of the index of refraction by measuring the absorption. For this reason, we set the value of the imaginary part of the complex index of refraction k_M, (k_I) for the metallic and (insulating) phase to the measured values, consistent with the values reported in the literature [36,37], and then use Eq. (4) and the measured value of R_M (R_I) in the metallic (insulating) phase to fix the corresponding value of n_M (n_I) (see Table I).

TABLE I. Comparative table between VO_2/TiO_2 and VO_2/Al_2O_3 sample parameters.

	VO_2/TiO_2	VO_2/Al_2O_3
$\langle T_c \rangle$	314.0 K	340.1 K
σ_{T_c}	2.6 K	8.8K
$\langle D \rangle$	17.4 nm	64.7 nm
$\langle D \rangle_{\mathrm{Exp}}$ [25]	13 nm	45 nm
σ_D	1.1 nm	38.5 nm
$n_M + ik_M$	$1.53 + i0.8$	$1.49 + i0.65$
R_M	0.14	0.11
$n_I + ik_I$	$3.03 + i0.57$	$2.60 + i0.60$
R_I	0.28	0.23
σ_K	1100 W/(K cm^2)	13 000 W/(K cm^2)

Using Eqs. (2)–(4), we can obtain the profile of $R(T)$ across the MIT for a given $P(T_c)$. Assuming $P(T_c)$ to be a Gaussian distribution, by fitting the measured profile of $R(T)$ to the one obtained using Eqs. (2)–(4) we can obtain the average value of the critical temperature $\langle T_c \rangle$ and its standard deviation σ_{T_c}. For VO_2/TiO_2 samples, we find $\langle T_c \rangle = 314$ K, $\sigma_{T_c} = 2.6$ K, for VO_2/Al_2O_3 samples $\langle T_c \rangle = 340$ K, $\sigma_{T_c} = 8.8$ K. The solid lines in Fig. 5 show the profiles of $R(T)$ obtained using Eqs. (2)–(4) and the above values for $\langle T_c \rangle$ and σ_{T_c}.

The difference in the value of T_c between VO_2/TiO_2 and VO_2/Al_2O_3 samples can be attributed to the fact that TiO_2, having a rutile structure, might induce strains into the VO_2 film that should favor the metallic phase of VO_2. In general, strain effects are expected to play an important role in the physics of the MIT phase transition of VO_2 films. In our approach, such effects enter indirectly, via the form of the probability distribution $P(T_c)$, and the value of the thermal conductivity of the interface between the VO_2 film and the substrate.

As we discuss in the following section, for our theoretical treatment of the recovery dynamics over long time scales of VO_2 films the knowledge of $P(T_c)$, i.e., $\langle T_c \rangle$ and σ_{T_c}, is all that is needed. As mentioned before, the fact that σ_{T_c} is nonzero is due to inhomogeneities, of different nature, present in the VO_2 film. It is practically impossible to know the distribution in the films of the properties affecting T_c. However, it is interesting to consider the limit in which the grain size D is the dominant property affecting T_c. The reason is that in this limit it is possible to extract, using strong and fundamental arguments, the distribution $P(D)$ for the grain size. In particular, it is possible to obtain the average grain size $\langle D \rangle$ and its standard deviation, quantities that are of great practical interest. $\langle D \rangle$ can be compared to estimates obtained using more direct experimental techniques, such as XRD. In the remainder of this section, we use the experimental results for $R(T)$ across the MIT to extract $\langle D \rangle$ and its standard deviation.

Theoretical and experimental evidence [38] indicates that for thin films the distribution $P(D)$ of the grain size D typically

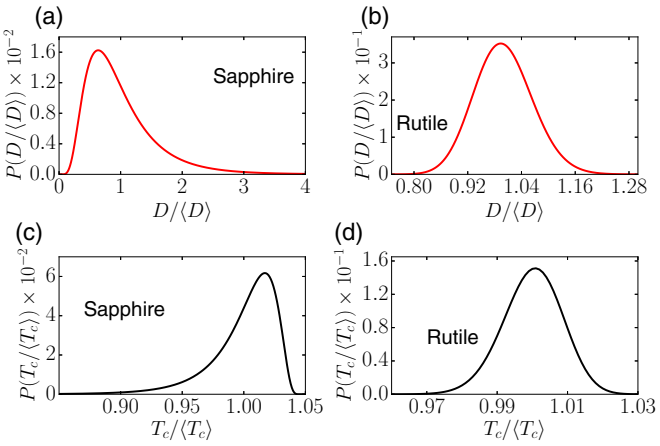

FIG. 6. (Color online) (a) and (b) show the grain size distributions normalized to the average grain size for sapphire ($\langle D\rangle = 64.7$ nm) and rutile ($\langle D\rangle = 17.4$ nm) substrates, respectively. (c) and (d) show the critical temperature distribution normalized to the average critical temperature for sapphire ($\langle T_c\rangle = 340.1$ K) and rutile ($\langle T_c\rangle = 314.0$ K), respectively. The bulk critical temperature is taken to be $T_c^{(\mathrm{bulk})} = 355$ K.

follows a logarithmic-normal distribution,

$$P(D) = \frac{1}{\sqrt{2\pi}\,\sigma\, D}\exp\left[-\frac{(\ln D/\hat{D})^2}{2\sigma^2}\right]. \tag{5}$$

In Eq. (5), D is the effective diameter of a grain, $\hat{D}$ is the grain size (diameter) such that $\ln\hat{D} = \langle \ln D\rangle$, and σ is the standard deviation of $\ln(D)$.

From general and fundamental arguments [39–42], we have

$$T_c = T_c^{(\mathrm{bulk})}\left(1 - \frac{1}{D/D_0}\right), \tag{6}$$

where $T_c^{(\mathrm{bulk})}$ is the bulk transition temperature and D_0, equal to 2 nm in our case, is the grain's diameter below which the grain is so small that is not possible to unambiguously identify its crystal structure. We set $T_c^{(\mathrm{bulk})} = 355$ K, that is the temperature above which the VO_2/Al_2O_3 sample is completely metallic. This value is higher than the value of bulk VO_2 due to the strain experienced by the films [27,28]. The relation between $P(D)$ and $P(T_c)$ is given by

$$P(T_c) = P(D(T_c))\frac{dD}{dT_c}. \tag{7}$$

Using Eqs. (2)–(7), by fitting the measured profile of $R(T)$ across the MIT, we can obtain $P(D)$ and therefore $\langle D\rangle$ and its standard deviation. Figures 6(a) and 6(b) show the profiles of $P(D)$ used to obtain the good theoretical fit to the evolution of $R(T)$ shown in Fig. 5. These profiles correspond to $\langle D\rangle = 64.7$ nm and $\sigma_D = 38.5$ nm for the VO_2/Al_2O_3 samples, and $\langle D\rangle = 17.4$ nm and $\sigma_D = 1.1$ nm for the VO_2/TiO_2 samples. It is interesting to compare the values of $\langle D\rangle$ obtained using this approach to the values estimated using XRD. From XRD data [25], we estimated $\langle D\rangle \approx 45$ nm for VO_2/Al_2O_3 and $\langle D\rangle \approx 13$ nm for VO_2/TiO_2 (see Table I). These values are in remarkable semiquantitative agreement with the values extracted from the profiles of $R(T)$ across

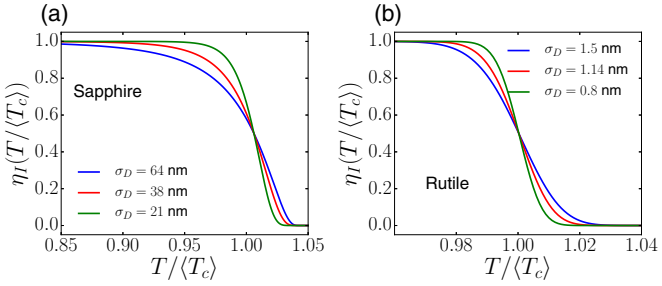

FIG. 7. (Color online) Evolution of the insulating partial volume η_I across the thermally induced MIT for case of (a) sapphire and (b) rutile substrates. For rutile, $\langle T_c\rangle = 314.0$ K and for sapphire $\langle T_c\rangle = 340.1$ K.

the MIT suggesting that the assumption that the grain size is the dominant property affecting the local value of T_c might be qualitatively correct. It is therefore interesting to obtain the profiles of $P(T_c)$ corresponding to the distributions of grain sizes shown in Figs. 6(a) and 6(b). Such profiles are shown in Figs. 6(c) and 6(d). The evolution of $\eta_I(T)$ across the MIT obtained using these profiles is shown in Fig. 7.

Our analysis suggest that the $R(T)$ profiles could be an indirect method to characterize the distribution of grain sizes in VO_2 films, a very challenging quantity to obtain using direct imaging experiments.

IV. THEORETICAL MODELING OF THE RELAXATION DYNAMICS OF THE MIT

In our experiment, the VO_2 films have a thickness d equal to or smaller than 110 nm (see Fig. 8), which is comparable with the laser $1/e$ penetration depth $\delta \simeq 110$–130 nm [25]. Thus we can assume that the pump pulse heats the film uniformly throughout its thickness. To describe the heat transfer process between the film and the substrate, we assume the temperature

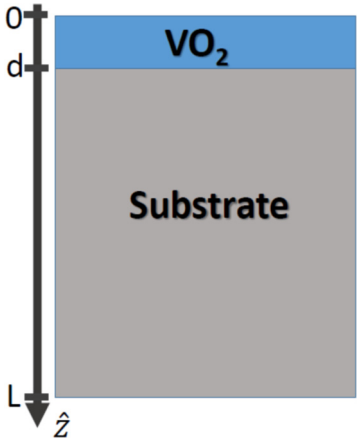

FIG. 8. (Color online) Sketch of the heterostructure considered in this work. It is composed of a vanadium dioxide (VO_2) thin film deposited on top of a substrate. The substrates considered in this work are titanium dioxide (TiO_2), and aluminum oxide (Al_2O_3). For VO_2/TiO_2, $d = 110$ nm while for VO_2/Al_2O_3, $d = 80$ nm. For both substrates, $L = 0.5$ mm.

to be uniform throughout the film for all times. Effectively, given these conditions, the heat transfer problem becomes a one-dimensional problem, and the equation for the rate of change of the heat (Q) in the film takes the form

$$\frac{dQ}{dt} = A \times d \times (\rho_I C_I \eta_I(T_f) + \rho_M C_M \eta_M(T_f) + L(T_f)P(T_f)\rho_{\text{av}})\frac{\partial T_f}{\partial t}, \quad (8)$$

where T_f is the film temperature, A is the area of the film, ρ_I (ρ_M) is the density in the insulating (metallic) phase, $\rho_{\text{av}} \equiv (\rho_I + \rho_M)/2$, C_I (C_M) is the heat capacity in the insulating (metallic) phase, L is the specific heat, and $P(T_f)dT_f$ is the fraction of the sample undergoing the MIT in the time interval dt during which the film temperature is in the interval $[T_f, T_f + dT_f]$. Here, $P(T_f)$ is the distribution of critical temperatures due to the inhomogeneities that we have obtained in the previous section. Using Eq. (2) and the fact that $\eta_M = (1 - \eta_I)$, we can rewrite Eq. (8) in a form that more explicitly shows the effect due to the inhomogeneities, i.e., the fact that the MIT is not characterized by a single T_c, but by a distribution of T_c's:

$$\frac{dQ}{dt} = A \times d \times \left[\rho_M C_M + (\rho_I C_I - \rho_M C_M)\int_{T_f}^{\infty} P(T_c)dT_c + L(T_f)P(T_f)\rho_{\text{av}}\right]\frac{\partial T_f}{\partial t}. \quad (9)$$

Equation (9) is the main result of our work: it allows to properly take into account the effect of inhomogeneities on the long time-scale dynamics across a first-order phase transition. The key quantity entering Eq. (9) is the distribution $P(T_c)$ that, as we have shown in the preceding section, can be obtained from the profile of $R(T)$ across the thermally activated MIT. Our work is the first to combine the information from the thermally activated MIT to obtain a physically accurate heat equation to describe the recovery dynamics after a photoinduced MIT.

For the latent heat, we have [39–41]

$$L = L^{(\text{bulk})}\frac{T_c}{T_c^{(\text{bulk})}}, \quad (10)$$

where $L^{(\text{bulk})}$ is the value of the specific heat for bulk VO_2. Given Eq. (6), Eq. (10) implies $L = L^{(\text{bulk})}(1 - D_0/D)$.

The rate of change of heat in the film given by Eq. (8) must be equal to the heat current (J_Q) across the interface between the film and the substrate:

$$J_Q = -\sigma_K A(T_f - T_s(d)), \quad (11)$$

where σ_K is the Kapitza constant characterizing the thermal conductivity of the interfaces [43–46], and $T_s(d)$ is the temperature of the substrate at the surface facing the VO_2 film. Combining Eqs. (9) and (11), for T_f, we obtain the equation

$$\left[\rho_M C_M + (\rho_I C_I - \rho_M C_M)\int_{T_f}^{\infty} P(T_c)dT_c + L(T_f)P(T_f)\rho_{\text{av}}\right]\frac{\partial T_f}{\partial t} = -\frac{\sigma_K}{d}(T_f - T_s(d)). \quad (12)$$

In Eq. (12), the only undetermined quantity is σ_K. We fix σ_K by fitting the theoretically obtained time evolution of $R(t)$ to the one measured experimentally, *for fixed experimental conditions* such as the temperature of the substrate and the pump fluence. The robustness of the theory presented is evidenced by the fact that, the same *fixed* value of σ_K provides a good agreement between the theoretical and the experimental results for a broad range of experimental conditions.

To completely define the problem, we need to supplement Eq. (12) with proper boundary conditions. The temperature distribution within the substrate, $T_s(z,t)$, satisfies the diffusion equation:

$$\frac{\partial T_s(z,t)}{\partial t} = \frac{k_s}{C_s \rho_s}\frac{\partial^2 T_s(z,t)}{\partial z^2}, \quad (13)$$

where k_s, C_s, ρ_s are the thermal conductivity, heat capacity, and mass density, respectively, of the substrate. The bottom of the substrate, for which $z = L$ (see Fig. 8), is kept at a fixed temperature $T_s^{(B)}$. At the film/substrate interface, the heat transferred from the film must be equal to the heat current $k_s \partial T_s/\partial z|_{z=d}$. We then have that the boundary conditions completing Eq. (13) are

$$T_s(z = L, t) = T_s^{(B)}; \quad (14)$$

$$k_s \left.\frac{\partial T_s(z,t)}{\partial z}\right|_{z=d} = -\sigma_K(T_f(t) - T_s(z = d, t)). \quad (15)$$

Equations (10) and (12)–(15), combined with knowledge of the distribution $P(T_c)$ completely define the temperature evolution of the VO_2 film. Notice that in these equations the only unknown parameter is the Kapitza constant σ_K. All the other quantities are known from direct measurements. $P(T_c)$ is obtained from the profile of $R(T)$ across the MIT, independently from the dynamics of R after the photoinduced insulator-to-metal transition. Also, the relation between the specific heat L and T is fixed by general and fundamental results [39–41].

While these equations can in general be solved only numerically, some qualitative understanding of the decay time τ can be gained if we make some simplifications. Let $P(T_c) = 1/(\sqrt{2\pi}\sigma_{T_c})\exp[-(T_c - \langle T_c\rangle)^2/(2\sigma_{T_c}^2)]$. At a temperature T, the insulating volume fraction is given by

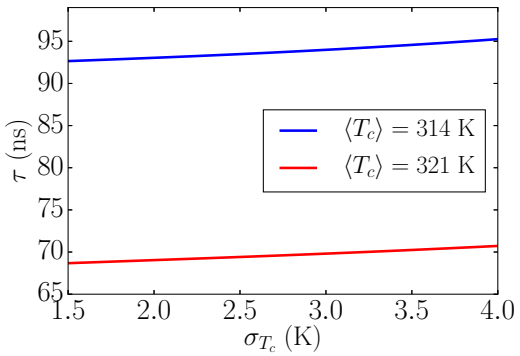

FIG. 9. (Color online) Full numerical calculation of the dependence of metal state decay constant τ on σ_{T_c} for two different values of the sample average critical temperature $\langle T_c\rangle$, and $T_s(L) = 280$ K. The initial temperature $T_0 = 360$ K is such that the sample is initially fully metallic, and $(T_0 - \langle T_c\rangle)/(\sqrt{2}\sigma_{T_c}) \approx 9$.

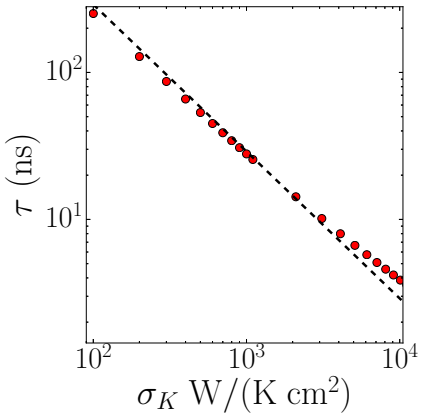

FIG. 10. (Color online) VO_2/Al_2O_3 metal state decay time τ dependence on the Kapitza constant σ_k for $\langle D\rangle = 64.7$ nm, $\sigma_D = 38.5$ nm, substrate temperature $T_s(L) = 310$ K, and fluence $\phi = 8\,\mathrm{mJ/cm^2}$. The red dots correspond to numerical calculations, and the dashed line is given by $\tau \propto \sigma_K^{-1}$.

$\eta_I(T) = \frac{1}{2}[1 - \mathrm{erf}((T - \langle T_c\rangle)/(\sqrt{2}\sigma_{T_c}))]$. Then assuming that the pump pulse is strong enough to drive the entire film into a fully metallic state at $t = 0$, the time dependence of the insulating volume fraction can be approximated by a simple exponential form $\eta_I(t) = 1 - Ae^{-t/\tau}$. In this case, an expression for the temperature can be obtained through the relationship $\eta_I(T(t)) = \eta_I(t)$. Furthermore, assuming that the substrate temperature T_s does not change with time, and the latent heat L to be temperature-independent, we can calculate the decay constant τ:

$$\tau = Cd\frac{\sigma_{T_c}}{\sigma_K}\frac{(C_M\rho_M + L\rho_{\mathrm{av}}P(T_0))}{T_0 - T_s} + \tau_0\,, \qquad (16)$$

where the constants $C > 0$, and τ_0 can only be determined by solving the full system of equations (12)–(15).

It is interesting to note that despite its many limitations, Eq. (16) captures many important qualitative traits of the actual relaxation process. For example, Fig. 9 shows a plot of the decay constant as a function of σ_{T_c} obtained solving the full system of equations (12)–(14) for two different values of the average critical temperature, and same initial temperature $T_0 = 360$ K. It is easy to see that the decay time τ follows the linear trend predicted by Eq. (16) in the limit $(T_0 - \langle T_c\rangle) \gg \sqrt{2}\sigma_{T_c}$. Similarly, an exact solution shows the inverse dependence of τ on the Kapitza constant, $\tau \propto \sigma_K^{-1}$, as shown in Fig. 10.

The relation (16) is another important result of our work, it shows how the characteristic time of the recovery dynamics is related to the properties of the VO_2 films. In particular, it shows the novel result that τ grows linearly with σ_{T_c}, the standard deviation of $P(T_c)$. σ_{T_c} can be reliably obtained from the profile of $R(T)$ across the MIT.

V. EFFECT OF INHOMOGENEITIES ON THE RELAXATION DYNAMICS OF THE PHOTOINDUCED MIT

Using the theoretical approach described in Sec. IV, we can obtain the time evolution of the optical reflectivity R through the MIT, as well as explain the significant difference in relaxation time scales between the two VO_2 samples

TABLE II. Parameters of VO_2 and substrates.

VO_2 heat capacity insulating phase C_I [47]	0.656 J/(g K)
heat capacity metallic phase C_M [47]	0.78 J/(g K)
density insulating phase ρ_I [46]	4.57 g/cm^3
density metallic phase ρ_M [46]	4.65 g/cm^3
thermal conductivity insulating phase κ_I [48]	3.5 W/(m K)
thermal conductivity metallic phase κ_M [48]	6 W/(m K)
bulk latent heat $L^{(\mathrm{bulk})}$ [47]	51.8 J/g
TiO_2 heat capacity C_s [49]	0.686 J/(g K)
density ρ_s [46]	4.25 g/cm^3
thermal conductivity κ_s [50]	8 W/(m K)
Al_2O_3 heat capacity C_s [51]	0.779 J/(g K)
density ρ_s [51]	3.98 g/cm^3
thermal conductivity κ_s [51]	30 W/(m K)
VO_2/TiO_2 absorption coefficient at 800 nm α [25]	0.01 nm^{-1}
VO_2/Al_2O_3 absorption coefficient at 800 nm α [25]	0.0076 nm^{-1}

considered. In all the numerical calculations, we assume C_I, ρ_I, C_M, and ρ_M to be equal to the bulk values for insulating and metallic VO_2, see Table II.

The initial film temperature is fixed by the pump fluence taking into account the Gaussian profile of the pulse and the fact that some of the heat is lost by the film during the time interval $[0,t_0]$ for which our analysis does not apply, $t = 0$ is time at which the pump pulse hits the VO_2 film and $t_0 = 10$ ns for VO_2/TiO_2 films and $t_0 = 0.5$ ns for VO_2/Al_2O_3 films.

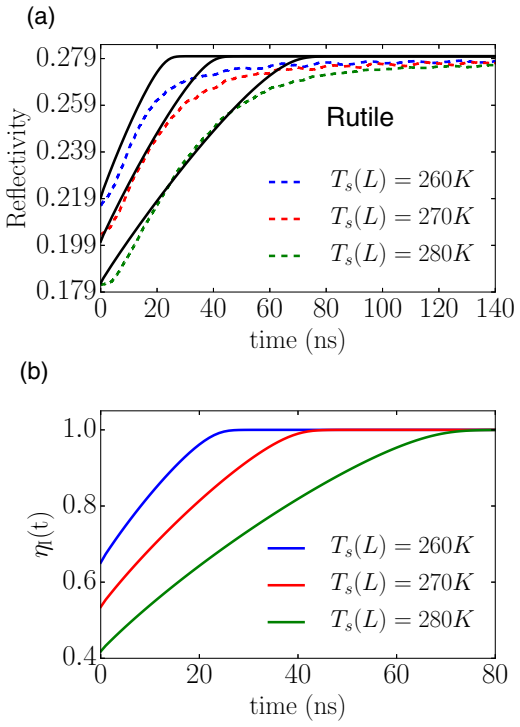

FIG. 11. (Color online) (a) Time evolution of reflectivity after the photoinduced MIT for VO_2/TiO_2 for three different $T_s(L)$ and $\phi = 9\,\mathrm{mJ/cm^2}$. The solid curves correspond to the theoretical results, and the dashed curves correspond to the experimental results. For the three theory curves, we use $\sigma_K = 1100\,\mathrm{W/(K\,cm^2)}$. (b) shows the corresponding insulating fraction time evolution.

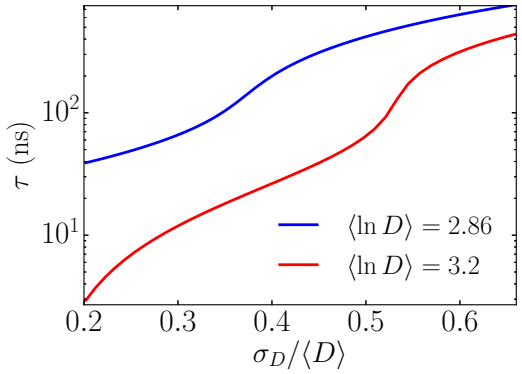

FIG. 12. (Color online) Dependence of the VO_2/TiO_2 metal state decay time constant τ on σ_D for two values of $\langle \ln D \rangle$, as defined in Eq. (5), Kapitza constant $\sigma_K = 1100\,\mathrm{W/(K\,cm^2)}$, substrate temperature $T_s(L) = 280$ K, and initial fluence $\phi = 9\,\mathrm{mJ/cm^2}$.

As discussed in Sec. IV, σ_K is the only unknown parameter. For the case of VO_2/TiO_2 samples, by fitting one of the curves for the dynamics of the reflectivity, we find $\sigma_K = 1100\,\mathrm{W/(K\,cm^2)}$. We find that all experimental curves are well approximated assuming the same value for the Kapitza constant, see Fig. 11(a). For the case of VO_2/Al_2O_3, the characteristic time scale of the recovery is much shorter than for VO_2/TiO_2 samples. As discussed in Sec. III, the two samples have very different inhomogeneities: σ_{T_c} is almost four times larger in VO_2/Al_2O_3 than VO_2/TiO_2. All other things being equal, Eq. (16) implies, see Fig. 12, that τ should be larger in VO_2/Al_2O_3 than in VO_2/TiO_2, the opposite of what is observed experimentally. We are then led to conclude that σ_K in VO_2/Al_2O_3 must be much higher than in VO_2/TiO_2. Figure 13 shows the measured evolution of R for the VO_2/Al_2O_3 sample for a fixed value of the fluence ϕ and substrate temperature, and the theoretical curves for this case that we obtain using the distribution $P(T_c)$ obtained for VO_2/Al_2O_3 and two different values of σ_K. We see that by choosing for σ_K the same value used for VO_2/TiO_2, there is no agreement between

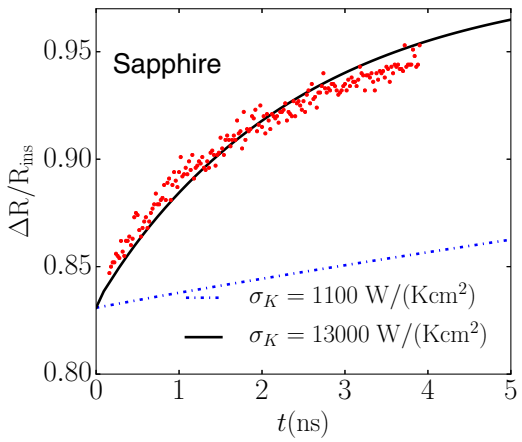

FIG. 13. (Color online) VO_2/Al_2O_3 reflectivity time evolution after photoinduced MIT for $\phi = 7.5\,\mathrm{mJ/cm^2}$. The red dots correspond to the experimental result. The dotted curve correspond to the theory with $\sigma_K = 1100\,\mathrm{W/(K\,cm^2)}$, and the solid curve corresponds to $\sigma_K = 13\,000\,\mathrm{W/(K\,cm^2)}$.

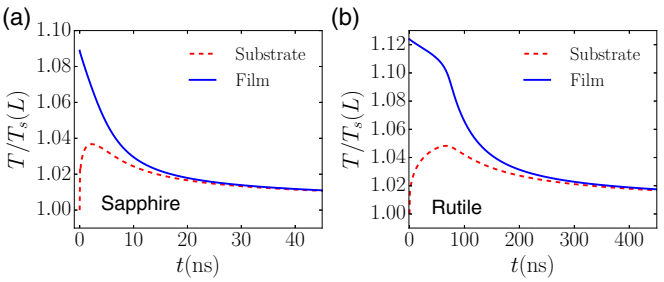

FIG. 14. (Color online) Film and substrate temperature time evolution. For sapphire (a), $T_s(L) = 310$ K, and for rutile (b), $T_s(L) = 280$ K.

theory and experiment. By setting $\sigma_K = 13\,000\,\mathrm{W/(K\,cm^2)}$, we obtain excellent agreement. Indeed, all the experimental curves $R(t)$ for VO_2/Al_2O_3 are well approximated by the theoretical results assuming $\sigma_K = 13\,000\,\mathrm{W/(K\,cm^2)}$.

Figure 14 shows the time evolution of the VO_2 film and substrate temperatures (close to the interface) for the VO_2/Al_2O_3 film, panel (a), and for the VO_2/TiO_2 film, panel (b), using the parameter values summarized in Table II. It helps to qualitatively understand the differences in the thermal relaxation between the two samples. Due to the lower values of the Kapitza constant, thermal energy stays more concentrated near the VO_2-TiO_2 interface, keeping the temperature of the VO_2 film above T_c longer.

To investigate the temperature dependence of the thermal relaxation, we repeated the measurements while changing the base substrate temperature of the VO_2/TiO_2 sample. For these measurements, the sample was placed inside a cryostat, and cooled down to temperatures $T_s(L)$ between 260 and 298 K. The results of these measurements, along with the theoretical calculations, are shown in Fig. 15. We again observe a good semiquantitative agreement between theoretical and experimental results. Also, note that the simple expression for the decay constant τ, Eq. (16), captures the overall decay rate drop at lower substrate temperatures $T_s(L)$.

We point out that all the theoretical curves are obtained using the fixed set of parameters shown in Table II. As mentioned above, the only unknown parameter that enters the theory is σ_K. In the results presented above, σ_K was fixed

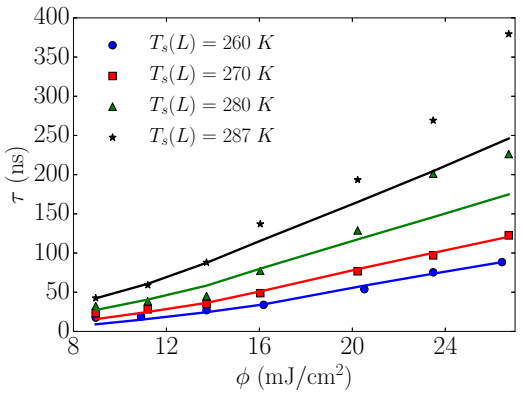

FIG. 15. (Color online) Dependence of metal state decay constant τ on fluence and substrate temperature for VO_2/TiO_2.

to a single value for each film, and this value was then used to obtain the results for a range of experimental conditions with different substrate temperatures and pump fluences. For example, Fig. 4 shows an excellent agreement between the experimental measurements and theoretical calculations across the entire range of pump fluences, limited on the lower end by our ability to reliably detect the variation in the probe reflectivity, and on the upper end by the damage threshold of our sample (pump fluence $>40\,\mathrm{mJ/cm^2}$).

VI. CONCLUSIONS

In conclusion, we have presented a combined experimental and theoretical study of the long time-scale recovery dynamics of VO_2 films following an ultrafast photoinduced insulator-to-metal transition. We have developed a theoretical approach that is able to properly take into account the effect of inhomogeneities. The main results of our work are (i) the derivation of the generalized heat equation (9) that properly takes into account that during the recovery, due to the inhomogeneities, only fraction of the sample is undergoing the metal-to-insulator transition and correctly tracks the evolution in time of the metallic (insulating) phase; (ii) the clarification of the connection between the temperature-dependent profile ($R(T)$) of the reflectivity across the thermally induced MIT and its dynamics after a photoinduced insulator-to-metal transition; (iii) the approximate relation, Eq. (16), between the characteristic time of the recovery dynamics and the parameters of the film, in particular to the standard deviation of the distribution of critical temperatures as extracted from $R(T)$; and (iv) the ability of our theory to describe, using a fixed value of the Kapitza constant, the recovery dynamics for different values of the substrate temperature and pump fluence. By changing the pump fluence the characteristic time of the recovery can be changed, experimentally, by two orders of magnitude: our theory is able to account for such a change.

The theoretical approach that we present is general and can be used to describe the dynamics (in the adiabatic limit) of inhomogeneous systems across a first order phase transition. The approximate relation between the characteristic time τ and the parameters of the system shows that τ is directly proportional to the width of the thermally activated transition. This result allows to estimate the recovery time of VO_2 films solely on the basis of a measurement of $R(T)$ across the MIT.

Assuming that variations of the size of the grains forming the films are the main source of inhomogeneities, using very general and fundamental relations between the grain size and the grain's critical temperature, we have been able to obtain the distribution of the grain sizes. In particular, we have been able to estimate the average grain's size and its standard deviation. We find that the calculated average grain's size is in remarkable semi-quantitative agreement with the one obtained from XRD measurements. For systems in which inhomogeneities are mostly due to variations of the size D of the grains, our analysis provides a way to obtain the size distribution $P(D)$ from the temperature dependent profile of the reflectivity across the thermally induced MIT. This could be very useful considering that $P(D)$ is a very challenging quantity to obtain via direct measurements.

ACKNOWLEDGMENTS

This work was funded in part by NSF, DMR-1006013: Plasmon Resonances and Metal Insulator Transitions in Highly Correlated Thin Film Systems, Jeffress Trust Awards program in Interdisciplinary Research, ONR-N00014-13-1-0321, and the NASA Virginia Space Grant Consortium. We also acknowledge support from the NRI/SRC sponsored ViNC center and the Commonwealth of Virginia through the Virginia Micro-Electronics Consortium (VMEC).

[1] F. J. Morin, Oxides Which Show a Metal-to-Insulator Transition at the Neel Temperature, Phys. Rev. Lett. **3**, 34 (1959).

[2] K. Sokolowski-Tinten, A. Cavalleri and D. Von Der Linde, Single-pulse time- and fluence-resolved optical measurements at femtosecond excited surfaces, Appl. Phys. A **69**, 577 (1999).

[3] A. Cavalleri, Cs. Tóth, C. W. Siders, J. A. Squier, F. Ráksi, P. Forget, and J. C. Kieffer, Femtosecond Structural Dynamics in VO_2 during an Ultrafast Solid-Solid Phase Transition, Phys. Rev. Lett. **87**, 237401 (2001).

[4] A. Cavalleri, Th. Dekorsy, H. Chong, J. Kieffer, and R. Schoenlein, Evidence for a structurally-driven insulator-to-metal transition in VO_2: A view from the ultrafast timescale, Phys. Rev. B **70**, 161102(R) (2004).

[5] A. Cavalleri, M. Rini, H. H. W. Chong, S. Fourmaux, T. E. Glover, P. A. Heimann, J. C. Kieffer, and R. W. Schoenlein, Band-Selective Measurements of Electron Dynamics in VO_2 Using Femtosecond Near-Edge X-Ray Absorption, Phys. Rev. Lett. **95**, 067405 (2005).

[6] H.-T. Kim, Y.-W. Lee, B.-J. Kim, B.-G. Chae, S. J. Yun, K.-Y. Kang, K.-J. Han, K.-J. Yee, and Y.-S. Lim, Monoclinic and Correlated Metal Phase in VO_2 as Evidence of the Mott Transition: Coherent Phonon Analysis. Phys. Rev. Lett. **97**, 266401 (2006).

[7] M. Nakajima, N. Takubo, Z. Hiroi, Y. Ueda, and T. Suemoto, Study of photo-induced phenomena in VO_2 by terahertz pump-probe spectroscopy, J. Lumin. **129**, 1802 (2009).

[8] T. L. Cocker, L. V. Titova, S. Fourmaux, H. C. Bandulet, D. Brassard, J. C. Kieffer, M. A. El Khakani, and F. A. Hegmann, Terahertz conductivity of the metal-insulator transition in a nanogranular VO_2 film, Appl. Phys. Lett. **97**, 221905 (2010).

[9] J. B. Goodenough, The two components of the crystallographic transition in VO_2, J. Solid State Chem. **3**, 490 (1971).

[10] A. Zylbersztejn and N. F. Mott, Metal-insulator transition in vanadium dioxide, Phys. Rev. B **11**, 4383 (1975).

[11] J. P. Pouget, H. Launois, J. P. D'Haenens, P. Merenda, and T. M. Rice, Electron Localization Induced by Uniaxial Stress in Pure VO_2, Phys. Rev. Lett. **35**, 873 (1975).

[12] V. Eyert, The metal-insulator transitions of VO_2: A band theoretical approach, Ann. Phys. **11**, 650 (2002).

[13] D. Paquet and P. Leroux-Hugon, Electron correlations and electron-lattice interactions in the metal-insulator, ferroelastic transition in VO_2: A thermodynamical study, Phys. Rev. B **22**, 5284 (1980).

[14] G Stefanovich, A Pergament, and D Stefanovich, Electrical switching and mott transition in VO_2, J. Phys.: Condens. Matter **12**, 8837 (2000).

[15] M. M. Qazilbash, M. Brehm, B. G. Chae, P. C. Ho, G. O. Andreev, B. J. Kim, S. J. Yun, A. V. Balatsky, M. B. Maple, F. Keilmann, H. T. Kim, and D. N. Basov, Mott transition in VO_2 revealed by infrared spectroscopy and nano-imaging, Science **318**, 1750 (2007).

[16] L. Wang, I. Novikova, J. M. Klopf, S. Madaras, G. P. Williams, E. Madaras, J. Lu, S. A. Wolf, and R. A. Lukaszew, Distinct length scales in the VO_2 metal-insulator transition revealed by bi-chromatic optical probing, Adv. Optical Mater. **2**, 30 (2014).

[17] M. F. Becker, A. Bruce Buckman, R. M. Walser, T. Lpine, P. Georges, and A. Brun, Femtosecond laser excitation of the semiconductor metal phase transition in VO_2, Appl. Phys. Lett. **65**, 1507 (1994).

[18] C. Kübler, H. Ehrke, R. Huber, R. Lopez, A. Halabica, R. F. Haglund, and A. Leitenstorfer, Coherent Structural Dynamics and Electronic Correlations during an Ultrafast Insulator-to-Metal Phase Transition in VO_2, Phys. Rev. Lett. **99**, 116401 (2007).

[19] D. J. Hilton, R. P. Prasankumar, S. Fourmaux, A. Cavalleri, D. Brassard, M. A. El Khakani, J. C. Kieffer, A. J. Taylor, and R. D. Averitt, Enhanced Photosusceptibility near T_c for the Light-Induced Insulator-to-Metal Phase Transition in Vanadium Dioxide, Phys. Rev. Lett. **99**, 226401 (2007).

[20] M. Rini, Z. Hao, R. W. Schoenlein, C. Giannetti, F. Parmigiani, S. Fourmaux, J. C. Kieffer, A. Fujimori, M. Onoda, S. Wall, and A. Cavalleri, Optical switching in VO_2 films by below-gap excitation, Appl. Phys. Lett. **92**, 181904 (2008).

[21] A. Pashkin, C. Kübler, H. Ehrke, R. Lopez, A. Halabica, R. F. Haglund, R. Huber, and A. Leitenstorfer, Ultrafast insulator-metal phase transition in VO_2 studied by multiterahertz spectroscopy, Phys. Rev. B **83**, 195120 (2011).

[22] E. Abreu, M. Liu, J. Lu, K. G West, S. Kittiwatanakul, W. Yin, S. A. Wolf, and R. D. Averitt, Thz spectroscopy of VO_2 epitaxial films: Controlling the anisotropic properties through strain engineering, New J. Phys. **14**, 083026 (2012).

[23] T. L. Cocker, L. V. Titova, S. Fourmaux, G. Holloway, H.-C. Bandulet, D. Brassard, J.-C. Kieffer, M. A. El Khakani, and F. A. Hegmann, Phase diagram of the ultrafast photoinduced insulator-metal transition in vanadium dioxide, Phys. Rev. B **85**, 155120 (2012).

[24] S. Wall, L. Foglia, D. Wegkamp, K. Appavoo, J. Nag, R. F. Haglund, J. Stähler, and M. Wolf, Tracking the evolution of electronic and structural properties of VO_2 during the ultrafast photoinduced insulator-metal transition, Phys. Rev. B **87**, 115126 (2013).

[25] E. Radue, L. Wang, S. Kittiwatanakul, J. Lu, S. A. Wolf, E. Rossi, R. A. Lukaszew, and I. Novikova, Substrate-induced microstructure effects on the dynamics of the photo-induced metal-insulator transition in VO_2 thin films, J. Opt. **17**, 025503 (2015).

[26] S. Lysenko, A. Rúa, V. Vikhnin, F. Fernández, and H. Liu, Insulator-to-metal phase transition and recovery processes in VO_2 thin films after femtosecond laser excitation, Phys. Rev. B **76**, 035104 (2007).

[27] D. Brassard, S. Fourmaux, M. Jean-Jacques, J. C. Kieffer, and M. A. El Khakani, Grain size effect on the semiconductor-metal phase transition characteristics of magnetron-sputtered VO_2 thin films, Appl. Phys. Lett. **87**, 051910 (2005).

[28] R. A. Aliev, V. N. Andreev, V. M. Kapralova, V. A. Klimov, A. I. Sobolev, and E. B. Shadrin, Effect of grain sizes on the metal-semiconductor phase transition in vanadium dioxide polycrystalline thin films, Phys. Solid State **48**, 929 (2006).

[29] K. G. West, J. Lu, J. Yu, D. Kirkwood, W. Chen, Y. Pei, J. Claassen, and S. A. Wolf, Growth and characterization of vanadium dioxide thin films prepared by reactive-biased target ion beam deposition, J. Vac. Sci. Technol., A **26**, 133 (2008).

[30] L. Wang, E. Radue, S. Kittiwatanakul, C. Clavero, J. Lu, S. A. Wolf, I. Novikova, and R. A. Lukaszew, Surface plasmon polaritons in VO_2 thin films for tunable low-loss plasmonic applications. Opt. Lett. **37**, 4335 (2012).

[31] E. Radue, E. Crisman, L. Wang, S. Kittiwatanakul, J. Lu, S. A. Wolf, R. Wincheski, R. A. Lukaszew, and I. Novikova, Effect of a substrate-induced microstructure on the optical properties of the insulator-metal transition temperature in VO_2 thin films, J. Appl. Phys. **113**, 233104 (2013).

[32] D. A. G. Bruggeman, Berechnung verschiedener physikalischer Konstanten von heterogenen Substanzen. I. Dielektriziäskonstanten und Leitfähigkeiten der Mischkörper aus isotropen Substanzen, Ann. Phys. **416**, 636 (1935).

[33] R. Landauer, The electrical resistance of binary metallic mixtures, J. Appl. Phys. **23**, 779 (1952).

[34] X. C. Zeng, D. J. Bergman, P. M. Hui, and D. Stroud, Effective-medium theory for weakly nonlinear composites, Phys. Rev. B **38**, 10970(R) (1988).

[35] E. Rossi, S. Adam, and S. Das Sarma, Effective medium theory for disordered two-dimensional graphene, Phys. Rev. B **79**, 245423 (2009).

[36] H. W. Verleur, A. S. Barker, Jr., and C. N. Berglund, Optical Properties of VO_2 between 0.25 and 5 eV, Phys. Rev. **172**, 788 (1968).

[37] J. B. Kana Kana, J. M. Ndjaka, G. Vignaud, A. Gibaud, and M. Maaza, Thermally tunable optical constants of vanadium dioxide thin films measured by spectroscopic ellipsometry, Opt. Commun. **284**, 807 (2011).

[38] C. G. Granqvist and R. A. Buhrman, Ultrafine metal particles, J. Appl. Phys. **47**, 2200 (1976).

[39] M. E. Fisher and A. N. Berker, Scaling for first-order phase transitions in thermodynamic and finite systems, Phys. Rev. B **26**, 2507 (1982).

[40] M. S. S. Challa, D. P. Landau, and K. Binder, Finite-size effects at temperature-driven first-order transitions, Phys. Rev. B **34**, 1841 (1986).

[41] M. Zhang, M. Yu. Efremov, F. Schiettekatte, E. A. Olson, A. T. Kwan, S. L. Lai, T. Wisleder, J. E. Greene, and L. H. Allen, Size-dependent melting point depression of nanostructures: Nanocalorimetric measurements, Phys. Rev. B **62**, 10548 (2000).

[42] Q. Jiang, J. C. Li, and B. Q. Chi, Size-dependent cohesive energy of nanocrystals, Chem. Phys. Lett. **366**, 551 (2002).

[43] P. L. Kapitza, The study of heat transfer in Helium II, J. Phys. USSR **4**, 181 (1941).

[44] G. L. Pollack, Kapitza Resistance, Rev. Mod. Phys. **41**, 48 (1969).

[45] R. Stoner and H. Maris, Kapitza conductance and heat flow between solids at temperatures from 50 to 300 K, Phys. Rev. B **48**, 16373 (1993).

[46] H. Wen, L. Guo, E. Barnes, J. H. Lee, D. A. Walko, R. D. Schaller, J. A. Moyer, R. Misra, Y. Li, E. M. Dufresne, D. G. Schlom, V. Gopalan, and J. W. Freeland, Structural and electronic recovery pathways of a photoexcited ultrathin VO_2 film, Phys. Rev. B **88**, 165424 (2013).

[47] C. N. Berglund and H. J. Guggenheim, Electronic properties of VO_2 near the semiconductor-metal transition, Phys. Rev. **185**, 1022 (1969).

[48] D.-W. Oh, C. Ko, S. Ramanathan, and D. G. Cahill, Thermal conductivity and dynamic heat capacity across the metal-insulator transition in thin film VO_2, Appl. Phys. Lett. **96**, 151906 (2010).

[49] D. de Ligny, P. Richet, E. F. Westrum, Jr., and J. Roux, Heat capacity and entropy of rutile (TiO_2) and nepheline ($NaAlSiO_4$), Phys. Chem. Minerals **29**, 267 (2002).

[50] W. R. Thurber and A. J. H. Mante, Thermal conductivity and thermoelectric power of rutile (Tio_2), Phys. Rev. **139**, A1655 (1965).

[51] V. Pishchik, L. A. Lytvynov, and E. R. Dobrovinskaya, *Sapphire: Material, Manufacturing, Applications*, 1st ed. (Springer, New York, 2009).